

Shared yet dissociable neural codes across eye gaze, valence and expectation

<https://doi.org/10.1038/s41586-020-2740-8>

Raviv Pryluk¹, Yosef Shohat¹, Anna Morozov¹, Dafna Friedman¹, Aryeh H. Taub¹ & Rony Paz¹✉

Received: 15 August 2019

Accepted: 25 June 2020

Published online: 23 September 2020

 Check for updates

The direction of the eye gaze of others is a prominent social cue in primates and is important for communication^{1–11}. Although gaze can signal threat and elicit anxiety^{6,12,13}, it remains unclear whether it shares neural circuitry with stimulus value. Notably, gaze not only has valence, but can also serve as a predictor of the outcome of a social encounter, which can be either negative or positive^{2,8,12,13}. Here we show that the neural codes for gaze and valence overlap in primates and that they involve two different mechanisms: one for the outcome and another for its expectation. Monkeys participated in the human intruder test^{13,14}, in which a human participant had either a direct or averted gaze, interleaved with blocks of aversive and appetitive conditioning. We find that single neurons in the amygdala encode gaze¹⁵, whereas neurons in the anterior cingulate cortex encode the social context¹⁶, but not gaze. We identify a shared population in the amygdala for which the neural responses to direct and averted gaze parallel the responses to aversive and appetitive stimulus, respectively. Furthermore, we distinguish between two neural mechanisms—an overall-activity scheme that is used for gaze and the unconditioned stimulus, and a correlated-selectivity scheme that is used for gaze and the conditioned stimulus. These findings provide insights into the origins of the neural mechanisms that underlie the computations of both social interactions and valence, and could help to shed light on mechanisms that underlie social anxiety and the comorbidity between anxiety and impaired social interactions.

Recognizing potentially harmful or beneficial stimuli is crucial for survival. In primates, facial expressions—and in particular the eye gaze of others—are prominent and highly instructive signals^{2–4,8,12}. Specifically, an averted or direct gaze is a social signal that can indicate submissive versus aggressive interactions, respectively. Indeed, gaze was shown to elicit anxiety in primates^{6,12,13}, and evokes responses in the amygdala^{15,17–19}—a brain region that serves as a hub for emotional responses in general and, in particular, in social contexts¹⁹. Moreover, gaze processing is disrupted in several neurodevelopmental and social disorders^{1,5,7,9,20}, for which abnormal activity of the amygdala is linked to gaze avoidance^{10,11}. Notably, gaze is not only a valence signal by itself, but also serves as a predictor of future outcomes: it can be aversive if an intruder maintains direct eye contact (stares), or it can potentially be rewarding if the other avoids eye contact. This is in line with the role of the amygdala not only in signalling outcome valence (appetitive or aversive), but also in learning through conditioning and signalling expectation for the outcome by responding to the conditioned stimulus (CS)^{21–24}. However, it remains unknown whether similar mechanisms are used for the coding of valence and eye gaze, and whether a shared coding for eye gaze and outcome expectation exists. Here we adapted the human intruder test (HIT)^{13,14}, a paradigm used to assess anxiety and defensive behaviours in non-human primates, and recorded the activity of single neurons in the amygdala and anterior cingulate cortex (ACC) during live interactions in a modified HIT paradigm that included an averted or direct gaze of the intruder and was combined with an

affective conditioning paradigm. We validated previous results and show that both the ACC and the amygdala encode valence²¹, whereas only the amygdala encodes gaze¹⁵. We also demonstrate that valence of both outcome and expectation are coded in the same ensemble of amygdala neurons that also encode the gaze of others, but through two different population codes.

Behaviour during eye-gaze and conditioning trials

Two monkeys participated in a modified version of the HIT (Fig. 1a). Each HIT block consisted of 18 interactions with a human intruder who is seated behind an LCD shutter (<1-ms response time), and who, when the shutter opens, either gazes directly at the eyes of the monkey (eye contact (EC)) or away from the monkey (averted gaze; that is, no eye contact (NEC)). These HIT blocks were interleaved with conditioning blocks of either appetitive or aversive trials (at least eight trials in a block) (Fig. 1b, c), in which the shutter opening serves as the conditioned stimulus (CS) and is followed after a 1-s delay by the outcome, or the unconditioned stimulus (US), which included either a liquid reward or an air puff in the appetitive or aversive blocks, respectively. We tracked the eye position of the monkeys and extracted four regions of interest (ROIs) (Fig. 1d): (1) the eye region of the intruder; (2) the face region of the intruder; (3) the whole shutter region; and (4) outside the shutter region. Oculomotor behaviour revealed distinct patterns (Fig. 1d–g and Extended Data Fig. 1): shutter opening in the HIT blocks

¹Department of Neurobiology, Weizmann Institute of Science, Rehovot, Israel. ✉e-mail: rony.paz@weizmann.ac.il

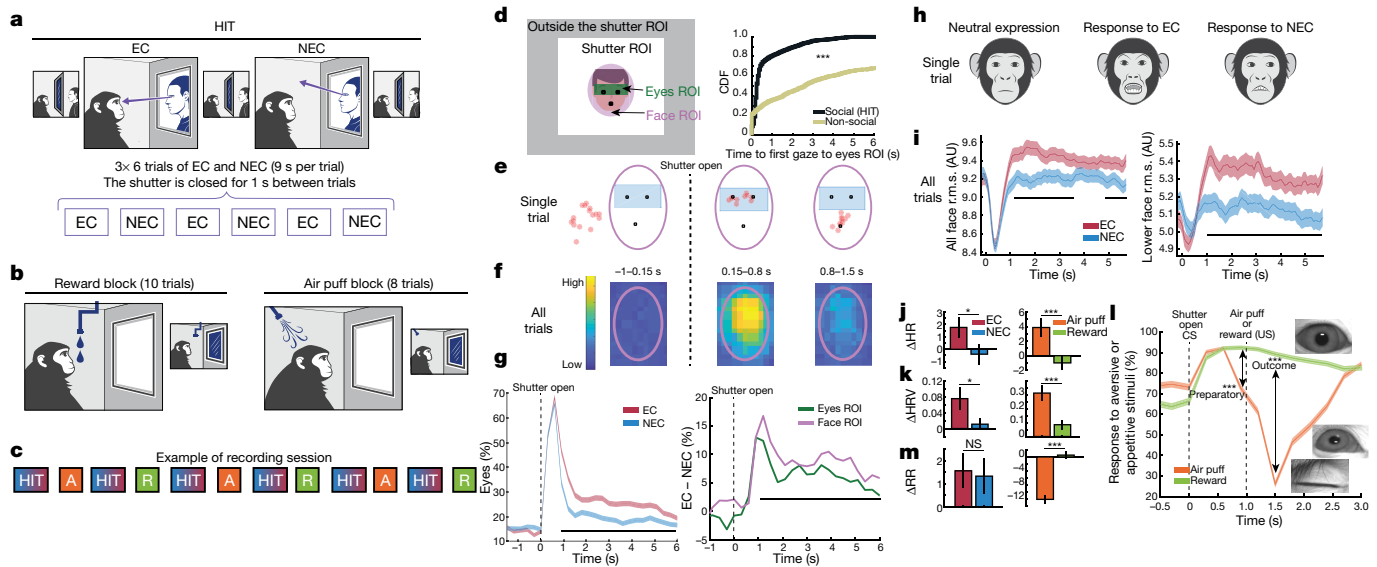


Fig. 1 | Behaviour during the HIT and affective-conditioning blocks. **a**, In the HIT analysis, the intruder pseudorandomly alters between a direct gaze (EC) and an averted gaze (NEC). Each block consists of a total of six alternating trials of EC and NEC (9 s per gaze; the shutter is closed for 1 s between trials); each block was repeated three times. **b**, Classical conditioning blocks of either appetitive (reward) or aversive (air puff) stimuli. Each appetitive block comprised 10 trials; each aversive block comprised 8 trials (20–40-s intertrial interval). Shutter open serves as a predictor (CS) for the appetitive or aversive outcome (US). **c**, An example of the pseudorandom order of blocks in one recording session. **d**, Left, ROIs for the eye tracking of the observer monkey. Green, the eyes; pink, the face; white, the whole shutter; grey, the whole possible space. Right, cumulative-density function (CDF) of the first time after shutter opening that the monkeys look into the eyes ROI, separately for HIT and for conditioning blocks. *** $P < 1 \times 10^{-8}$; Kolmogorov–Smirnov test; $n_{\text{trials}} = 3,108$ HIT and 2,090 conditioning trials; 49 sessions, 24 or 25 sessions per monkey. **e**, Example of one shutter opening in an HIT block. Filled circles (red) mark the location of the monkey's gaze overlaid on the real position of the intruder (schematic). **f**, Density function of all eye locations in the HIT blocks in the same three consecutive time windows as in **e**. Immediately after shutter opening and for few hundreds of milliseconds, the monkey looks mainly at the eyes of the human intruder. **g**, Left, percentage of time looking to the eyes ROI. Data are mean \pm s.e.m. Right, the difference in the percentage of time that the monkey

looks at the eyes and face ROIs between EC and NEC trials. The black line indicates a significant difference ($P < 0.05$); χ^2 test; $n = 1,480$ NEC trials and 1,628 EC trials. **h**, Schematics of typical facial expressions made by the monkeys in EC trials (middle, ‘aggressive’), in NEC trials (right, ‘interest’), compared with a neutral expression (left). **i**, The overall change in the facial expression in EC and NEC. Data are mean \pm s.e.m. The root-mean-square (r.m.s.) of change in the image over the whole face (left) and only for the lower half of the face (right), compared with the neutral expression. The black line represents a significant difference ($P < 0.05$); two-sided Student's t -test; $n = 1,480$ NEC and 1,628 EC trials (Methods and Extended Data Fig. 2). **j**, Differences in heart rate (ΔHR) between EC and NEC trials (left) and between reward and air puff trials (right). Data are mean \pm s.e.m.; two-sided Student's t -test; * $P < 0.05$, *** $P < 1 \times 10^{-3}$, $n = 1,703$ NEC and 1,765 EC trials; *** $P < 1 \times 10^{-3}$, $n = 1,352$ reward and 712 air puff trials. **k**, Differences in heart-rate variability (ΔHRV) between EC and NEC trials (left) and between reward and air puff trials (right). Data are mean \pm s.e.m.; two-sided Student's t -test; * $P < 0.05$, *** $P < 1 \times 10^{-3}$. **l**, Response to aversive (air puff) or appetitive (reward) in oculomotor behaviour. Data are mean \pm s.e.m.; χ^2 test; *** $P < 1 \times 10^{-3}$, $n = 1,375$ reward and 715 air puff trials. **m**, Differences in respiratory rate (RR) after the shutter opens between EC and NEC trials (left) and between reward and air puff trials (right). Data are mean \pm s.e.m.; two-sided Student's t -test; NS, not significant ($P = 0.82$), $n = 1,703$ NEC and 1,765 EC trials; *** $P < 1 \times 10^{-3}$, $n = 1,352$ reward and 712 air puff trials.

induced more interest in the eyes ROI compared to the conditioning blocks (Kolmogorov–Smirnov test; $P < 1 \times 10^{-8}$; $n = 3,108$ HIT and 2,090 conditioning trials; 49 sessions, 24 or 25 sessions per monkey) (Fig. 1d). After exploring the eyes of the human intruder, the monkeys continued to look more towards the eyes and face ROIs in blocks of direct gaze (EC versus NEC, χ^2 test, $P < 1 \times 10^{-3}$) (Fig. 1g). We further aligned each trial separately according to the first time the monkey looked at the intruder eyes (interquartile range, 180–700 ms) and found similar results (χ^2 test, $P < 1 \times 10^{-6}$) (Extended Data Fig. 1).

We quantified the facial expressions that were elicited by the appearance of an intruder and found that monkeys produced more facial expressions when the intruders made eye contact (χ^2 test, $P < 1 \times 10^{-2}$) (Fig. 1h, i and Extended Data Fig. 2), in agreement with the stressful, threatening and defensive responses that are traditionally induced by the direct gaze of a human intruder¹³. Heart rate and heart-rate variability further suggest that the monkeys showed anxiety-related responses (Student's t -test, $P < 0.05$) (Fig. 1j, k). In the conditioning blocks, the monkeys quickly learned to distinguish and anticipate the different outcomes (appetitive or aversive) after shutter opening in each specific block (χ^2 test, $P < 1 \times 10^{-3}$) (Fig. 1l). In aversive (air puff) blocks, the monkeys closed their eyes after the shutter opened both in preparation of the air puff as well as immediately after its delivery (χ^2 test, $P < 1 \times 10^{-3}$)

(Fig. 1l). In addition, they did not inhale before the expected air puff, but did before reward (Student's t -test, $P < 1 \times 10^{-3}$) (Fig. 1m). The heart rate and heart-rate variability in conditioning blocks were different between air puff and reward trials (Student's t -test, $P < 1 \times 10^{-3}$) (Fig. 1j, k) and had the same direction of modulation as in the HIT trials (air puff and EC trials have higher changes in heart rate and heart-rate variability than reward and NEC trials, respectively).

Therefore, there were different behavioural responses in HIT sessions to eye contact or no eye contact of the intruder, and there was a differential response between appetitive and aversive blocks, for both the outcome (US) and the expectation (CS).

Responsive neurons in the amygdala and ACC

To examine neural responses, we recorded single units from the basolateral complex of the amygdala and the ACC (Fig. 2a) ($n = 24$ or 25 sessions per monkey; $n = 356$ and 203 neurons in the ACC and amygdala, respectively; 224 and 103, and 132 and 100, neurons in the ACC and amygdala, respectively, were recorded per monkey). We defined two epochs in the conditioning blocks: a preparatory or expectation epoch (CS-related, after the shutter opened but before the US delivery) and an outcome epoch (US-related, after the delivery of the air puff or reward)

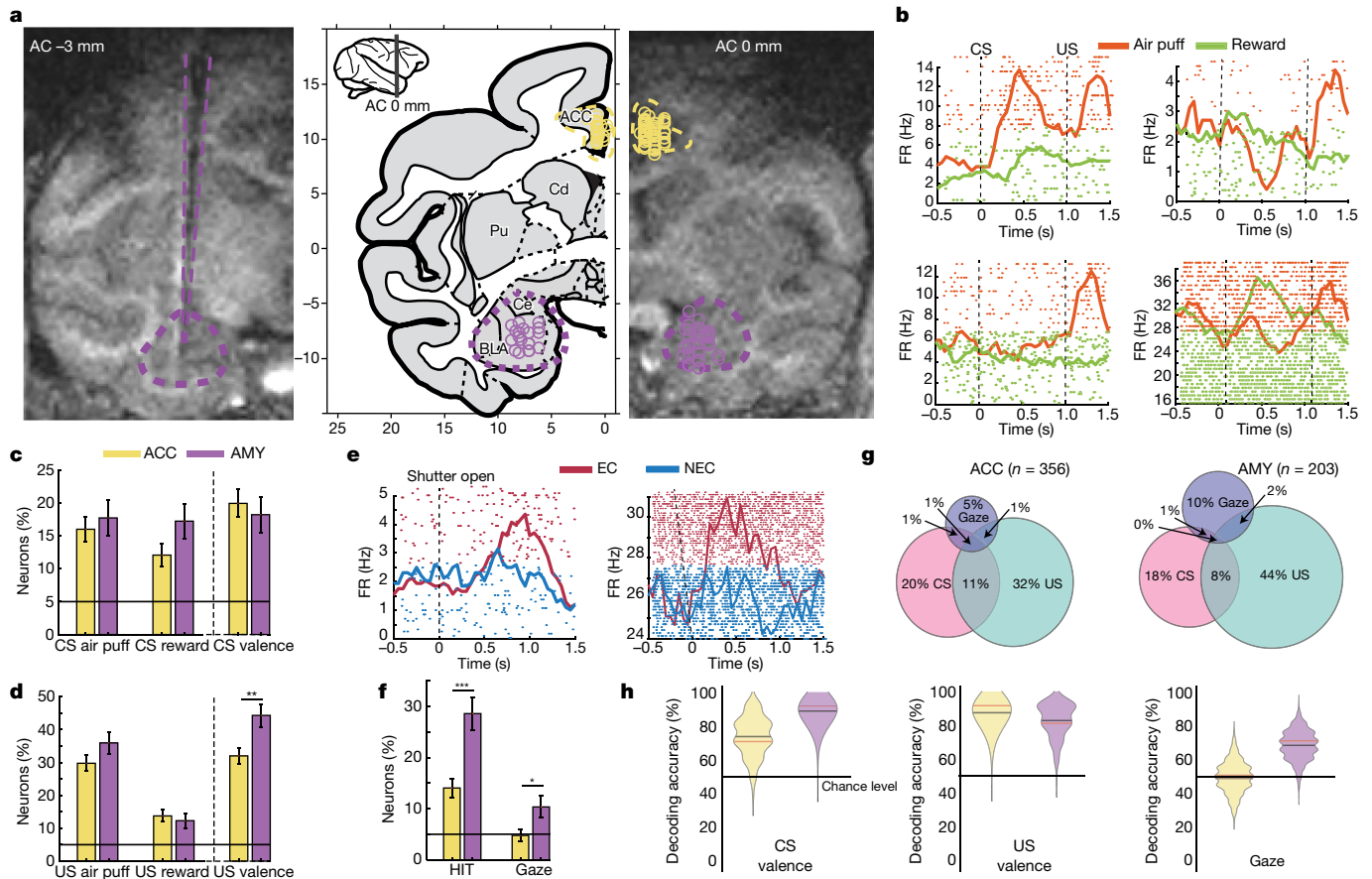


Fig. 2 | The amygdala encodes gaze and valence, and the ACC mainly encodes valence. **a**, Left, the recording location is shown on an MRI with the electrode directed into the basolateral complex of the amygdala (AC = -3), Middle and right, recording locations overlaid on a primate brain map (AC = 0) and on an MRI scan (AC = 0). Pu, putamen; Cd, caudate nucleus; Ce, central amygdala; BLA, baso-lateral complex of the amygdala. **b**, Peristimulus time histograms overlaid on raster plots of two representative neurons in the ACC and two in the amygdala during conditioning block. FR, firing rate. **c**, The percentage of neurons in the ACC ($n = 356$ neurons) and the amygdala (AMY; $n = 203$ neurons) that responds to the CS (shutter open) in aversive trials (left), appetitive trials (middle) and that discriminate between the two (right). Data are mean \pm s.e.m. **d**, The percentage of neurons in the ACC and in the amygdala that respond after the US to the air puff (left), reward (middle) and that

discriminate between the two (right). Data are mean \pm s.e.m.; χ^2 test; ** $P < 1 \times 10^{-2}$. **e**, Peristimulus time histograms overlaid on raster plot of two representative neurons in the amygdala during the HIT. **f**, The percentage of neurons in the ACC and the amygdala that respond significantly in the HIT blocks, and that discriminate between EC and NEC (gaze neurons). Data are mean \pm s.e.m.; χ^2 test; * $P < 0.05$; *** $P < 1 \times 10^{-3}$. **g**, Overlaps in the number of neurons that responds across the different tasks. The size is proportional to the percentage of neurons. **h**, Population decoding accuracy for HIT versus conditioning blocks. Significance above chance level (black line) was tested using bootstrap analysis. In all comparisons except ACC gaze, accuracies were significantly above chance. Data are mean (black thin line), median (red line) and 95% confidence intervals. $n = 1,000$ bootstrap replicates, $n = 356$ ACC neurons, $n = 203$ amygdala neurons.

(Fig. 2b). As expected, neurons in both regions responded to the appetitive CS (amygdala, 35 out of 203 neurons; ACC, 43 out of 356 neurons; χ^2 test, $P < 1 \times 10^{-3}$ for both), responded to the aversive CS (amygdala, 36 out of 203 neurons; ACC: 57 out of 356 neurons; χ^2 test, $P < 1 \times 10^{-3}$ for both) and discriminated between valence (amygdala, 37 out of 203 neurons; ACC, 71 out of 356 neurons; χ^2 test, $P < 1 \times 10^{-3}$) (Fig. 2c). Similar proportions of neurons responded in both regions (χ^2 test, $P > 0.09$ for all). Similarly, neurons in the ACC and in the amygdala responded to the appetitive US (amygdala, 25 out of 203 neurons; ACC, 49 out of 356 neurons; χ^2 test, $P < 1 \times 10^{-2}$) and aversive US (amygdala, 73 out of 203 neurons; ACC, 106 out of 356 χ^2 test, $P < 1 \times 10^{-3}$) with similar proportions (χ^2 test, $P > 0.1$). However, more amygdala neurons discriminated valence between appetitive and aversive outcomes (amygdala, 90 out of 203 neurons; ACC, 114 out of 356 neurons; χ^2 test, $P < 1 \times 10^{-2}$) (Fig. 2d).

In the HIT blocks (Fig. 2e), responses were computed from the time when the monkey first looked at the eyes ROI, as this is the time point at which the monkey could differentiate EC from NEC trials (interquartile range, 180–700 ms) (Fig. 1d). More amygdala neurons responded during HIT blocks (amygdala, 58 out of 203 neurons; ACC, 50 out of

356 neurons; χ^2 test, $P < 1 \times 10^{-3}$) (Fig. 2f), and more amygdala neurons discriminated EC from NEC trials (amygdala, 21 out of 203 neurons; ACC, 17 out of 356 neurons, χ^2 test, $P < 0.05$; the ACC was not different from chance level; binomial test, $P > 0.1$) (Fig. 2f). There was little overlap in the neurons that responded to both gaze and valence in both regions (binomial test, $P > 0.1$) (Fig. 2g).

Consistent with previous studies¹⁵, the proportion of amygdala neurons that responded to gaze was low compared with the proportion that responded to valence, both for CS- and US-related responses (χ^2 test; CS, $P < 0.05$; US, $P < 1 \times 10^{-3}$) (Fig. 2c, d, f). Nevertheless, as a neuron can contribute at the population level even if it does not exhibit a significant response, we further tested whether the combined ensemble holds information about the eye gaze of others by training a linear decoder on population vectors. In accordance with the single-cell analyses, population activity in the amygdala and ACC could discriminate appetitive from aversive trials, using either CS- or US-related activity (bootstrap analysis with 95% confidence intervals) (Fig. 2h). However, only the amygdala population discriminated EC from NEC, and the ACC population did not (bootstrap analysis with 95% confidence interval)

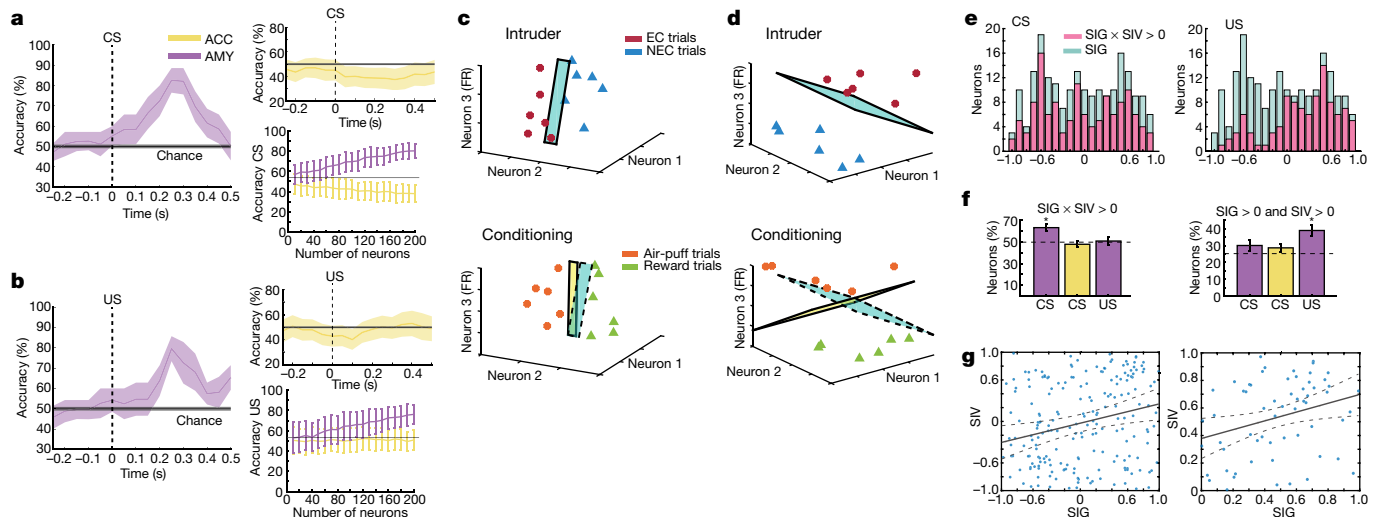


Fig. 3 | Shared coding for valence and gaze in amygdala neurons.

a, Population decoding accuracy in the amygdala (left) and ACC (top right) when training on eye gaze (EC versus NEC) and testing on valence (aversive versus appetitive) using CS-related activity. Bottom right, peak decoding accuracy using increasing numbers of neurons. Data are mean \pm s.d., $n=1,000$ bootstrap replicates. **b**, Same as **a** in for US-related activity. **c**, The correlated-selectivity scheme. Neurons respond similarly to gaze and valence. Top, the optimal linear separator for the neural population (demonstrated here for three neurons) during the HIT trials. Bottom, a similar presentation is shown for the conditioning experiment, overlaid with the separating surface from the HIT experiment (cyan). The similar surfaces enable correct decoding. **d**, Same as **c** for the overall-activity scheme. Different neurons in the population respond with similar changes in firing rate to gaze and valence, but individual neurons are not correlated. Although the separating surfaces are different, neurons provide enough spikes overall to enable correct decoding. **e**, Distribution of the selectivity index for gaze (SIG; blue), overlaid with

neurons that have the same direction of modulation for selectivity index for gaze and selectivity index for valence (SIV; red), for CS activity (left) and US activity (right). The ACC is shown for comparison. The dashed line is chance level. Data are mean \pm s.e.m.; χ^2 test; $P<1\times 10^{-3}$ (CS versus chance). Right, percentage of neurons in the amygdala for which positive indices are higher than chance in US only, but not in CS. The ACC is shown for comparison. The dashed line is chance level. Data are mean \pm s.e.m.; χ^2 test; $P<1\times 10^{-3}$ (US versus chance). **g**, Left, the selectivity index (SI) for gaze is correlated with the selectivity index for valence across the whole population only during CS activity ($r=0.26$, $P<0.01$ taking only classically selective neurons with SI > 1/3; $r=0.2$, $P<0.01$ for the whole population; US, $P>0.4$; two-sided Student's t -tests). Right, the correlation holds when considering only positive indices ($r=0.3$, $P<0.02$, Pearson's correlation; US, $P>0.4$; two-sided Student's t -tests), demonstrating that the correlation is beyond only the sign.

(Fig. 2h). We conclude that the amygdala and the ACC encode valence²¹, but only the amygdala encodes the eye gaze of the intruder¹⁵, both at the single-cell and population level.

Shared population activity in the amygdala

The finding that the amygdala holds information about valence as well as eye gaze within the same circuitry suggests that there might be a shared population code. To test this hypothesis, we used the decoder approach but this time trained the algorithm on one type of trials and tested on the other. If discrimination accuracy is above chance level, this would mean that the population uses similar mechanisms to hold information for one situation (that is, appetitive or aversive) as for the other (that is, NEC or EC).

In agreement with the aforementioned finding that the ACC does not hold information about eye gaze, the decoding performance in the ACC was not different from chance in both CS- and US-related activity (bootstrap analysis with 95% confidence interval) (Fig. 3a, b). By contrast, decoding performance was significantly above chance level when using the amygdala population, and it was true when using either CS- or US-related activity (bootstrap analysis with 95% confidence interval) (Fig. 3a, b and Extended Data Fig. 3). Performance was approximately linear in the number of neurons, starting at chance level and increasing to more than 80% accuracy when using all available neurons (CS, 82.5%; US, 80%; $n=203$, $P<0.001$ for both) (Fig. 3a, b). This finding suggests that the shared coding is not due to the few neurons that respond to both contexts (Fig. 2g), which is further supported by the similar accuracy when these neurons are removed from the analyses (CS, 81%, $n=201$; US, 79%, $n=198$). These findings demonstrate that a shared population code is used by amygdala neurons.

Dissociable schemes for gaze, valence and expectation

We examined two shared activity schemes that would enable us to train the algorithm on one context and to decode the other. In the first scheme—termed correlated selectivity—neurons respond similarly to gaze and valence (Fig. 3c). That is, neurons respond in the same direction and with a similar proportion; the response of a neuron shows a direct correlation between eye gaze and valence. In the second—termed overall activity—a population of neurons respond in the same direction, meaning that there is an overall change in the firing rate, but that individual neurons are not correlated across the contexts (Fig. 3d). We tested which scheme applies here and whether it is different between CS- and US-related activity.

We first examined the activity at the single-cell level. Each neuron was assigned a selectivity index for gaze (from -1 to 1 for NEC and EC) and a selectivity index for valence (from -1 to 1 for appetitive to aversive). The joint distribution of indices with the same direction of modulation was high during the CS period (χ^2 test, $P<1\times 10^{-3}$; compared with chance level; US, $P>0.1$) (Fig. 3e, f), in contrast to the joint distribution with only positive modulation, which was high in the US period (χ^2 test, $P<1\times 10^{-3}$; CS, $P>0.1$) (Fig. 3e, f). Moreover, the two indices were correlated across the whole population only during CS activity ($r=0.26$, $P<0.01$ when taking only neurons with a selectivity index of more than 1/3; and $r=0.2$, $P<0.01$ for the whole population; US, $P>0.4$; Student's t -tests), and this correlation was retained when taking only the positive indices, demonstrating that the correlation is associated with more than the sign of the index ($r=0.3$, $P<0.02$; US, $P>0.4$) (Fig. 3g).

Next, we used linear regression on the individual responses separately for gaze and valence. We obtained and compared the following two coefficients: β_{valence} represents the difference in firing rate between

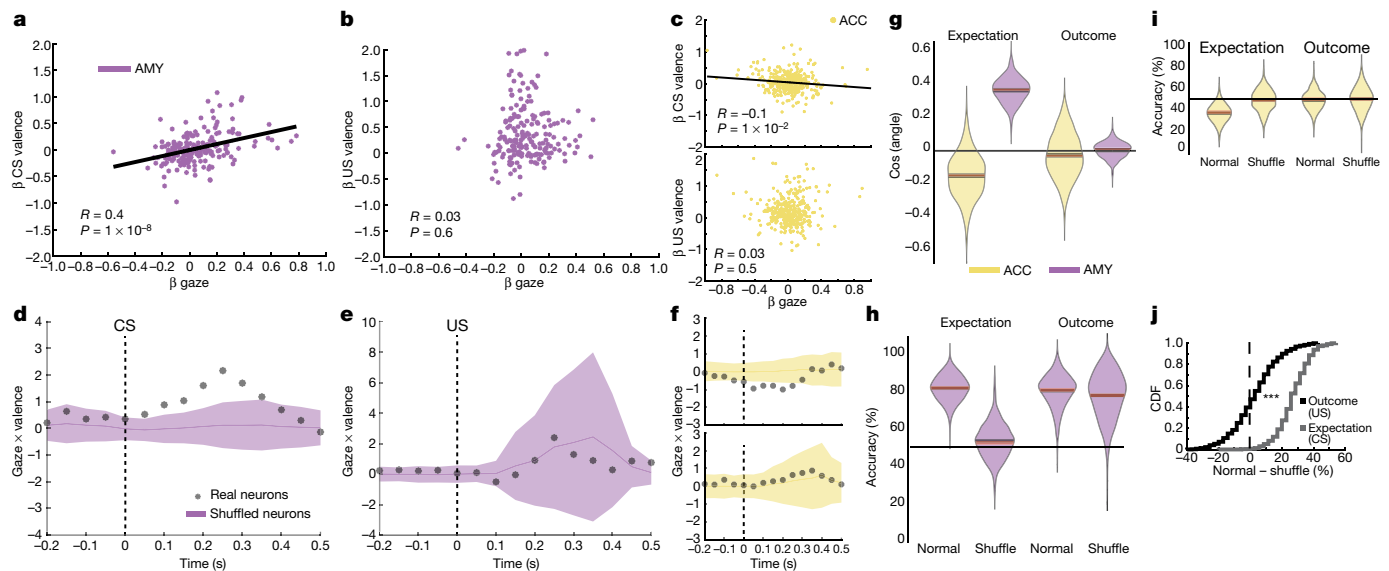


Fig. 4 | An overall-activity coding for eye gaze and US valence and a correlated-selectivity coding for eye gaze and CS valence. **a**, Correlation (Pearson's) between the linear-regression coefficients of gaze (x axis) and valence (y axis) in the amygdala using CS-related activity. All amygdala neurons are shown. The β values are from the time epochs of the maximal decoding from Fig. 3. **b**, Same as **a** using US-related activity in the amygdala. **c**, Same as **a** and **b** for CS-related (top) and US-related (bottom) activity in the ACC. **d**, Neurons respond in the same direction for eye gaze and valence using CS-related activity in the amygdala, as evident by the scalar product between the coefficients of gaze and valence for each neuron. Black symbols represent

data from real neurons and magenta shading is the 95% confidence interval based on bootstrap shuffling of the data. **e**, Same as **d** using US-related activity in the amygdala. **f**, Same as **c** and **d** for CS-related (top) and US-related (bottom) activity in the ACC. **g**, The angle between the decision boundaries derived from the population vector of gaze and valence separately. The scalar product is shown. **h**, Population decoding accuracy for real and shuffled neurons using CS-related and US-related activity in the amygdala. **i**, Same as **h** for CS-related and US-related activity in the ACC. **j**, Cumulative distribution of the difference in decoding accuracy between real and shuffled neurons of the amygdala. *** $P < 1 \times 10^{-3}$; two-sample Kolmogorov–Smirnov test.

air puff and reward trials; β_{gaze} represents the difference in firing rate between EC and NEC. If the two coefficients were similar for individual neurons, it indicates that neurons encode valence and eye gaze not only in the same direction, but also with a similar modulation. Consistent with the selectivity-index analysis, we found that the two coefficients were positively correlated in amygdala neurons, but only when CS-related activity was used, not when US-related activity was used (Pearson's correlation; amygdala: CS, $r = 0.4$, $P < 1 \times 10^{-8}$; US, $r = 0.03$, $P > 0.5$; ACC: CS, $r = -0.1$, $P < 1 \times 10^{-2}$; US, $r = 0.03$, $P > 0.5$) (Fig. 4a–c). This observation supports a correlated-selectivity scheme between valence and gaze for the CS epoch, but an overall-activity scheme for the US epoch. The overall-activity scheme for the US epoch was further supported by direct examination of overall increases and decreases in firing rates for direct gaze and US valence (z -test, $P < 1 \times 10^{-3}$) (Extended Data Fig. 4).

This finding was further validated by examining the scalar product between the vectors of the two coefficients (β_{gaze} and β_{valence}). If more neurons respond with a similar proportion (correlated selectivity), then the scalar product would be positive; otherwise, the scalar product will be close to zero if neurons responded in random order (or negative if in opposite directions). In the amygdala, using CS-related activity outperformed a shuffling test using bootstrap analysis (Fig. 4d); however, using US-related activity did not (Fig. 4e). In the ACC, the performance of neurons was similar to or lower than the shuffled test (Fig. 4f). In addition, the mean value of the US-related shuffled activity was higher than that of the CS-related shuffled activity (CS = 0.1, US = 1.8; bootstrap analysis, $P < 0.05$) (Fig. 4d, e). This was because more neurons that encoded gaze or US valence increased their firing rate, which results in a higher positive scalar product for shuffled neurons; these results further support the overall-activity scheme for the US epoch. By contrast, the similarity in the CS-related response to gaze response increased the scalar product in the real neurons but not in the shuffled population.

To test the two schemes at the population level, we computed the angles between the decision boundaries of two linear decoders: one that separates EC from NEC trials and one that separates aversive from appetitive trials. When computed over the US epoch, or using the ACC population, the decision boundaries of valence and gaze were closer to being perpendicular to one another (with a dot product that was not significantly different from zero), whereas only using CS activity from the amygdala population shows a significant difference from perpendicular decision boundaries (bootstrap, 95% confidence interval) (Fig. 4g).

Finally, we trained the decoder on gaze and tested on valence while shuffling the order of neurons. Consistent with the results described above, performance using amygdala activity from the CS epoch was decreased markedly when using shuffled neurons compared with the performance of real neurons (bootstrap analysis with 95% confidence interval) (Fig. 4h–j and Extended Data Fig. 5), whereas using US activity performance with shuffled neurons was slightly increased compared with the performance of real neurons (bootstrap analysis with 95% confidence interval) (Fig. 4h–j and Extended Data Fig. 5), further supporting the two different shared coding schemes: correlated selectivity between gaze and CS valence, and overall activity between gaze and US valence.

Conclusions

The eyes of others became a prominent signal during evolution owing to anatomical changes in the facial morphology that forced a shift in salience from the shape of the face to the eyes². The importance of the amygdala in the processing of eye gaze has been shown in primates^{10,15,17}. Here we recorded neural activity in the amygdala and ACC during live interactions in a modified version of the HIT¹³ that also included a conditioning paradigm. Whereas both regions differentiated between valence²¹, only the amygdala differentiated between the gaze of an intruder. This finding is consistent with the

multidimensional selectivity that is found in amygdala neurons^{25,26} and the increased robustness compared with the ACC²⁷. Notably, we found that in the amygdala, both CS- and US-related responses were shared with the eye gaze of the intruder in a valence-specific manner—that is, aversive (air puff) or appetitive (reward) responses were in parallel with a direct or averted eye gaze, respectively. Our results, in which aversive-to-appetitive responses paralleled the responses to natural eye gaze, suggest that social value evolved from, or parallel to, primary reinforcer value. Together with recent findings²⁸, our results further support the idea that the processing of social stimuli and—specifically—eye gaze does not occur in separate dedicated neural circuits^{2,29}.

The naturalistic paradigm that we used enabled live social interactions, which are important for the interpretation of natural behaviours; however, it also imposed some constraints. We therefore validated that our findings could not be explained by differences that associated the direct or averted eye gaze, such as vocalizations (of any type, Extended Data Fig. 6a), self-motor activity (Extended Data Fig. 6b), facial expressions (Extended Data Fig. 6c–e), saccades (Extended Data Fig. 1b) and stimulus saliency (Extended Data Figs. 7–10). The fact that we identified two different coding schemes argues against the possibility that the shared code reflects a general saliency and/or category code (Extended Data Figs. 7, 8). This was further supported by control experiments that showed that amygdala neurons encode species differences¹⁸, yet this encoding was not shared with the outcome expectation (Extended Data Fig. 9). Furthermore, additional experiments demonstrated that a direct or averted gaze has different values compared with neutral trials (Extended Data Fig. 10).

We identified two different schemes that enabled the decoding of value based on responses to eye gaze. The overall-activity scheme that was shared across gaze and outcome (US) occurs through an overall non-specific increase in firing rate and points to a mechanism with origins within the same circuitry, suggesting that an aversive outcome is similar in value to a predator gaze¹² or to a threat from a peer. This is also in line with the findings of the HIT in which gaze elicits anxiety^{6,13,30}. The coding of expectation, namely the learned CS, was also shared with eye-gaze responses, but it was shared through a correlated-selectivity scheme that requires the responses to be correlated at a single-neuron level (rather than only on average over the population). Because correlated selectivity could require a more-specific wiring design, and because the amygdala has evolved in parallel to the development of social interactions^{31,32}, we suggest that this scheme could have facilitated the later evolution of other complex social processes such as learning by observation and social-based decision-making in extended circuits^{9,16,33–35}. Specifically, it can be used by the primate to anticipate social outcomes based on context—a direct prolonged gaze probably calls for a challenge and predicts a confrontation that entails a dangerous outcome; whereas an averted gaze usually predicts a submissive and permissive encounter and can potentially be rewarding (mating or the sharing or offering of food). There are very few contexts in which a prolonged gaze is positive (for example, in mother–baby interactions), and it will be interesting to examine whether amygdala ensembles reverse coding direction, or contribute to the integration of cues in other circuits.

Our findings offer insights into coding schemes in the primate amygdala that underlie social interactions, valence and outcome expectancy and provide a framework to understand social anxiety and the comorbidity of anxiety, depression and impaired social interactions²⁰.

Online content

Any methods, additional references, Nature Research reporting summaries, source data, extended data, supplementary information,

acknowledgements, peer review information; details of author contributions and competing interests; and statements of data and code availability are available at <https://doi.org/10.1038/s41586-020-2740-8>.

- Jones, W. & Klin, A. Attention to eyes is present but in decline in 2–6-month-old infants later diagnosed with autism. *Nature* **504**, 427–431 (2013).
- Emery, N. J. The eyes have it: the neuroethology, function and evolution of social gaze. *Neurosci. Biobehav. Rev.* **24**, 581–604 (2000).
- Gobel, M. S., Kim, H. S. & Richardson, D. C. The dual function of social gaze. *Cognition* **136**, 359–364 (2015).
- Adolphs, R. Neural systems for recognizing emotion. *Curr. Opin. Neurobiol.* **12**, 169–177 (2002).
- Zhou, Y. et al. Atypical behaviour and connectivity in SHANK3-mutant macaques. *Nature* **570**, 326–331 (2019).
- Schneier, F. R., Kent, J. M., Star, A. & Hirsch, J. Neural circuitry of submissive behavior in social anxiety disorder: a preliminary study of response to direct eye gaze. *Psychiatry Res.* **173**, 248–250 (2009).
- Schneier, F. R., Rodebaugh, T. L., Blanco, C., Lewin, H. & Liebowitz, M. R. Fear and avoidance of eye contact in social anxiety disorder. *Compr. Psychiatry* **52**, 81–87 (2011).
- Ballesta, S. & Duhamel, J. R. Rudimentary empathy in macaques' social decision-making. *Proc. Natl Acad. Sci. USA* **112**, 15516–15521 (2015).
- Gariépy, J. F. et al. Social learning in humans and other animals. *Front. Neurosci.* **8**, 58 (2014).
- Rutishauser, U. et al. Single-neuron correlates of atypical face processing in autism. *Neuron* **80**, 887–899 (2013).
- Hadjikhani, N. et al. Look me in the eyes: constraining gaze in the eye-region provokes abnormally high subcortical activation in autism. *Sci. Rep.* **7**, 3163 (2017).
- Shepherd, S. V. Following gaze: gaze-following behavior as a window into social cognition. *Front. Integr. Neurosci.* **4**, 5 (2010).
- Kalin, N. H. & Shelton, S. E. Defensive behaviors in infant rhesus monkeys: environmental cues and neurochemical regulation. *Science* **243**, 1718–1721 (1989).
- Oler, J. A. et al. Amygdala and hippocampal substrates of anxious temperament differ in their heritability. *Nature* **466**, 864–868 (2010).
- Mosher, C. P., Zimmerman, P. E. & Gothard, K. M. Neurons in the monkey amygdala detect eye contact during naturalistic social interactions. *Curr. Biol.* **24**, 2459–2464 (2014).
- Haroush, K. & Williams, Z. M. Neuronal prediction of opponent's behavior during cooperative social interchange in primates. *Cell* **160**, 1233–1245 (2015).
- Gamer, M. & Büchel, C. Amygdala activation predicts gaze toward fearful eyes. *J. Neurosci.* **29**, 9123–9126 (2009).
- Gothard, K. M., Battaglia, F. P., Erickson, C. A., Spitler, K. M. & Amaral, D. G. Neural responses to facial expression and face identity in the monkey amygdala. *J. Neurophysiol.* **97**, 1671–1683 (2007).
- Adolphs, R. What does the amygdala contribute to social cognition? *Ann. NY Acad. Sci.* **1191**, 42–61 (2010).
- Stein, M. B. & Stein, D. J. Social anxiety disorder. *Lancet* **371**, 1115–1125 (2008).
- Tovote, P., Fadok, J. P. & Lüthi, A. Neuronal circuits for fear and anxiety. *Nat. Rev. Neurosci.* **16**, 317–331 (2015).
- Heroy, C. & Johansen, J. P. Encoding of fear learning and memory in distributed neuronal circuits. *Nat. Neurosci.* **17**, 1644–1654 (2014).
- Davarci, S. & Pare, D. Amygdala microcircuits controlling learned fear. *Neuron* **82**, 966–980 (2014).
- Janak, P. H. & Tye, K. M. From circuits to behaviour in the amygdala. *Nature* **517**, 284–292 (2015).
- Putnam, P. T. & Gothard, K. M. Multidimensional neural selectivity in the primate amygdala. *eNeuro* **6**, ENEURO.0153-19.2019 (2019).
- Kyriazi, P., Headley, D. B. & Pare, D. Multi-dimensional coding by basolateral amygdala neurons. *Neuron* **99**, 1315–1328 (2018).
- Pryluk, R., Kfir, Y., Gelbard-Sagiv, H., Fried, I. & Paz, R. A tradeoff in the neural code across regions and species. *Cell* **176**, 597–6098 (2019).
- Munuera, J., Rigotti, M. & Salzman, C. D. Shared neural coding for social hierarchy and reward value in primate amygdala. *Nat. Neurosci.* **21**, 415–423 (2018).
- Dunbar, R. I. M. The social brain hypothesis. *Evol. Anthropol.* **6**, 178–190 (1998).
- Myllyneva, A., Ranta, K. & Hietanen, J. K. Psychophysiological responses to eye contact in adolescents with social anxiety disorder. *Biol. Psychol.* **109**, 151–158 (2015).
- Bickart, K. C., Wright, C. I., Dautoff, R. J., Dickerson, B. C. & Barrett, L. F. Amygdala volume and social network size in humans. *Nat. Neurosci.* **14**, 163–164 (2011).
- Sallet, J. et al. Social network size affects neural circuits in macaques. *Science* **334**, 697–700 (2011).
- Dal Monte, O., Chu, C. C. J., Fagan, N. A. & Chang, S. W. C. Specialized medial prefrontal–amygdala coordination in other-regarding decision preference. *Nat. Neurosci.* **23**, 565–574 (2020).
- Grabenhorst, F., Baez-Mendoza, R., Genest, W., Deco, G. & Schultz, W. Primate amygdala neurons simulate decision processes of social partners. *Cell* **177**, 986–998 (2019).
- Allsop, S. A. et al. Corticoamygdala transfer of socially derived information gates observational learning. *Cell* **173**, 1329–1342 (2018).

Publisher's note Springer Nature remains neutral with regard to jurisdictional claims in published maps and institutional affiliations.

© The Author(s), under exclusive licence to Springer Nature Limited 2020

Methods

Data reporting

No statistical methods were used to predetermine sample size. The experiments were not randomized and the investigators were not blinded to allocation during experiments and outcome assessment.

Animals and surgical procedures

Two male *Macaca fascicularis* (4–8 kg) were implanted with a round recording chamber above the amygdala and ACC covering both regions in both hemispheres. All procedures were approved and conducted in accordance with the regulations of the Weizmann Institute Animal Care and Use Committee (IACUC), following NIH regulations and with AAALAC accreditation.

MRI based electrode positioning scans were acquired twice, on a 3-Tesla MRI scanner (MAGNETOM Trio, Siemens) with a CP knee coil (Siemens) and using 0.53 mm resolution. A first scan before surgery was used to align and refine anatomical maps for the individual monkeys (relative location of the amygdala, ACC and anatomical markers such as the interaural line and the anterior commissure), and to guide the positioning of the chamber on the skull. After surgery, we performed scans with deep electrodes directed towards the amygdala and the ACC (Fig. 2a), and calculated the anatomical anterior–posterior and lateral–medial borders relative to the penetrations. The depth of the amygdala is calculated from the dura surface.

Electrophysiology recordings

Each day, 1–3 multichannel (16 contacts each) microelectrodes vector arrays (NeuroNexus) were lowered into the brain using an electrode-positioning system (NAN). Vectors were moved independently into the amygdala and ACC while identifying electrophysiological markers tracking the known anatomical pathway. We allowed 30 min for the tissue and signal to stabilize before starting acquisition and the behavioural protocol. Data are pre-amplified and stored at 22 kHz for later processing. In real time, a 0.3 Hz–6 kHz band-pass filter was applied and online spike sorting was performed using a template-based algorithm (Alpha Lab Pro, Alpha Omega). Offline spike sorting was performed on the raw data for all sessions to improve unit isolation (offline sorter, Plexon).

Behavioural paradigms

A fast LCD shutter (307 mm × 407 mm) was placed between the monkey and the intruder (FOS-307 × 406-PSCT-LV; Liquid Crystal Technologies) to block the visual site. Direct current (48 V) through the LCD shutter turned it clear/transparent with an onset/offset rise time of <1 ms. To enhance the precision of neural activity we placed a photodiode (BPX65 Silicon PIN Photodiode) that could be detected with onset/offset of <110⁻⁴ ms. There were three types of blocks in each daily session: HIT; air puffs; liquid rewards. The blocks were randomized during a session, with more than 120 s separating blocks (Fig. 1).

Reward. Each block contained 10 trials with an inter-trial interval of a pseudorandom 20–40 s. In each trial, the shutter opening served as the CS and was followed after a 1-s delay by few drops of juice delivered to the mouth of the monkey.

Air puff. Each block contained 8 trials with an inter-trial interval of a pseudorandom 20–40 s. In each trial, the shutter opening served as the CS and was followed after a 1-s delay by an air puff (5–15 Psi; located 5 cm from the face).

HIT. Each block included 6 × 3 shutter openings, in which the human intruder alternated between EC and NEC in a pseudorandom order. In both EC and NEC trials, the human maintained the gaze direction for 6–9 s independently of the behaviour of the monkeys. We generated

a per-day predefined sequence of EC and NEC with three options of sequences that altered across sessions: sequence 1 (block A, EC, NEC, EC, NEC, EC, NEC; block B, EC, EC, NEC, EC, EC; block C, NEC, NEC, EC, EC, NEC, EC); sequence 2 (blocks B, C, A) and sequence 3 (blocks C, A, B). This was aimed to randomize and prevent learning of the EC/NEC order, but also to provide across-days statistics for neural recordings. The face of the human intruder was filmed and all trials were monitored to validate that the intruders indeed maintained a constant gaze and followed the daily sequence.

The monkeys had information about which block was about to start as the human intruder paradigm started with 5 s of pure sinus wave (300 Hz) followed by the human intruder entering the room and sitting in front of the monkey, with closed shutter. The monkey could not see any part of the human unless the shutter was open.

Behavioural analysis

Eye tracking. A stationary monocular eye tracker was installed for the purpose of eye tracking and gaze estimation. The system included two cameras (Ximea_MQ013RG)—one for capturing the eyes of the monkey and one to monitor the gaze of the human intruder—and an infrared LED light bar (MetaBright Exolight ISO-14-IRN-24) for face illumination and production of corneal reflection. The eye-recording camera efficiently captured the corneal reflection due to its near-infrared property.

Software implementation was based on the open-source project ‘OpenEyes’³⁶, which enables the estimation of the point of gaze of the participant on the projection of the field of view. In our case, images of the field of view scene were extracted from the video stream of the intruder monitoring camera. The conditions of our experimental setup (brightly lighted room, large corneal reflection of near-rectangular shape and brown sclera of the monkey) required a slight modification of the original algorithm for pupil and detection of the corneal reflection. In our variation of the software, the shot-noise reduction was skipped, and the corneal reflection was not removed from the image after its detection, due to its large size. To find the pupil centre, we extended the Starburst algorithm. After finding the feature candidates for pupil contour, instead of fitting an ellipse using the RANSAC (random sample consensus) paradigm, we used the ‘imfindcircles’ MATLAB function, which searches for circle candidates by applying a Hough-transform-based algorithm. To generate the input for the function, an edges image was produced by gradient magnitude calculation followed by binarization. This procedure resulted in a black image with white edges, and was passed to ‘imfindcircles’ with the object polarity parameter set to ‘dark’ (specifying that the object—the pupil—is darker than its background). The function returned a list of candidate circles, ordered by circle strengths. Starting from the circle with the largest strength, the list is searched for the first circle that contained a predefined number of minimum feature points that were extracted by the Starburst algorithm. Finally, the pupil centre was estimated by the centre of the found circle. A standard calibration procedure was performed, whereby the monkeys sequentially fixated on 3 × 3 known grid points in the scene image (according to the original OpenEyes implementation). To cause the fixation of the gaze of the monkey, the screen with the shutter closed, was consecutively illuminated by a laser pointer in the nine locations. The exact frames of the fixation of the gaze were detected and coordinated with the illumination timings (each time that the laser is activated, it records the exact time in the system). The human intruders were filmed throughout all of the interactions with the monkeys, and their faces and eyes were marked both automatically and manually for validation. The nine (3 × 3) fixation points were filmed by the same camera, allowing the projections of the fixation points and the intruders on the same plane. Each frame of the eyes of the monkeys therefore resulted in a point (x and y position) on this plane, allowing us to calculate the gaze of the monkey in one of the four ROIs—eyes of the intruders, face of the intruders, shutter region and the rest of the view.

Facial expression. One Ximea_MQ013RG camera filmed the face region of the recoded monkey at 34 Hz. For every recording session, the mean image during the ‘alone’ period was calculated (that is, when the monkey was alone in the room with closed shutter). This mean image (Extended Data Fig. 2) was subtracted from every frame taken during the interactions with the human intruder. The r.m.s. of all the pixels in this subtracted frame is then calculated and the mean and s.e.m. are presented for EC and NEC trials (Fig. 1i). Additionally, each day we manually define 3 ROIs: upper face, lower face and ears (Extended Data Fig. 2). The same analysis was repeated separately for each ROI and differences between EC and NEC were validated across both upper and lower face (Fig. 1i and Extended Data Fig. 2).

Heart-rate and respiratory-rate measurements. The cardiac and respiratory traces (to measure the heart rate, heart-rate variability and respiratory rate)³⁷ were recorded using a piezoelectric pulse transducer (UFI, model 1010) at 2,790 Hz. We use an elastic belt about 23 cm (9 inches) long and fastened an extender belt to one end of the transducer package using VELCRO closures that were all wrapped around the chest of the monkey. We use a piezoelectric pulse transducer (UFI, model 1010) glued around the centre to directly sense the heart pulse.

For validation, the respiratory trace was also recorded using a solid-state transducer, which measures changes in chest or abdominal circumference due to respiration (UFI, model 1132) at 2,790 Hz. The signal from the piezo sensor also provides respiratory-rate parameters, allowing two independent measures for comparison and calibration of parameters.

The piezo-electric signal was processed using custom-made MATLAB software. A respiratory trace was extracted using a first-order Butterworth filter and smoothed with running windows. Respiratory peaks were then extracted using the ‘findpeaks’ function. A cardiac trace was extracted by subtracting the filtered respiratory signal from the raw piezo-electric signal. The resulting signal was then processed for each day separately, using filtering and findpeaks parameters. The parameters of the day-specific processing were derived by comparing different sets of parameters to manually tagged cardiac peaks from each day. The resulting day-tailored processed signal was validated using manual inspection of all trials. In addition, the quality of each trial was manually rated, and noisy signal epochs were marked to validate that the result was not due to trials of insufficient quality.

Respiratory-rate and heart-rate measurements were calculated for each trial using a sliding window of 1 s and heart-rate variability was calculated using running window of 5 s, yielding a continuous signal for further analysis. The heart-rate variability measure is the standard deviation of the normal–normal beat interval. Finally, we normalized the changes in each measure by subtracting the mean value from the closed shutter epoch before each trial, to obtain evoked responses.

Vocalizations. Vocalizations were recorded using a microphone (PGA81, Cardioid Condenser Instrument Microphone), situated in close proximity to the monkey. The signal was processed using custom-made MATLAB software implementing a first-order Butterworth filter and smoothed with running a window. Threshold detection was implemented after subtracting the background noise. Several thresholds were tested (1, 2, 3 or 4 s.d.) and the conclusions remain similar.

Movement detection. Two accelerometers were used in the experiment (EVAL-ADXL335Z, Analogue Devices), one was attached to the chair of the monkey and one to the setup itself. This allowed us to differentiate between acceleration caused by self-motor movements and other environmental noise. Movements were recorded at 2,790 Hz and processed using custom-made MATLAB software implementing a first-order Butterworth filter and smoothed with a running window. Peaks were then extracted using the findpeaks function.

Comparing conditions. We implemented a control based on the thinning method, traditionally used to compare distributions from different sources. Here, we compared the distribution of facial expressions or eye gaze in EC versus NEC trials. We created similar distributions of facial expressions (eye movements) for EC and NEC trials, and repeated the main analysis.

Neural activity analysis

Single-neuron analysis. The analysis of the neural data focused on three time epochs. In the human intruder blocks, we focused on 400–700 ms after shutter opening. This time epoch was chosen because of the oculomotor behaviour of the monkeys (Fig. 1), which showed that the first time they can identify whether this is an EC or an NEC trial has an interquartile range of 180–700 ms (see Fig. 1d for the full cumulative-density function). All analyses were repeated (Extended Data Figs. 1, 5) when aligning each trial according to the actual time in that trial that the EC/NEC information was available (first gaze to eyes ROI). Such an alignment was done to focus on the differences between the EC and NEC of the intruder and because fixation shapes neural activity¹⁵. In the affective (reward/aversive) conditioning blocks, the neural data were taken from 0 to 300 ms after the CS, termed CS-related activity; and from 0 to 300 ms after reward/air puff delivery (US), termed US-related activity.

Neural activity was normalized according to the baseline activity before the relevant block, using the same window length (300 ms) to calculate the mean and s.d. of the firing rate.

Therefore, the normalized (z-scored) firing rate (FR) was:

$$FR_{\text{normalized}} = \frac{FR - \text{mean}_{\text{baseline}}}{\text{s.d.}_{\text{baseline}}}$$

These z-scores were used to quantify the percentage of responsive neurons to the different stimuli. Student’s *t*-tests were used to compare valence (air puff to reward) or gaze (EC or NEC), and χ^2 or binomial tests were used to compare the percentage of responsive neurons.

Population decoding. A pseudo-simultaneous population response vector was used for the decoding analysis. This procedure has been described in detail elsewhere³⁸. The population vector contained spike counts of each neuron in a specific time bin. Each brain area had its own vectors, and the number of vectors was defined by the number of available trials:

$$PV(t) = \langle \text{Neuron}_1^C, \text{Neuron}_2^C, \dots, \text{Neuron}_N^C \rangle$$

$PV(t)$ was the response vector of a specific trial in condition *C*, in time bin (*t*), in a brain region that had *N* neurons. We used the same number of neurons in the amygdala and ACC, therefore we randomly discarded excess neurons in the ACC, resulting in 203 neurons in both.

There were four conditions: air puff and reward belong to the valence class, and EC and NEC belong to the gaze class. In the analysis that was performed in Fig. 2, we trained and tested within the same class, whereas in all other analyses we trained on one class and tested on the other class. If we changed the order in the training, such that training for NEC yielded air puff and training for EC yielded reward, the decoding accuracy was the same (100 – CorectDecoding) (Extended Data Fig. 3). For both the training and testing we used a linear classifier based on maximization procedure of the SVM algorithm (the fitSVM MATLAB function). Each training set yielded a boundary line (set of weights for every neuron) and a threshold that separated the two conditions under consideration. The same output from the training was then used to assess the accuracy in the test set.

For a given neuron and a given condition, we used 80% of the trials for training and 20% for testing when done within the same class. When we

trained on one class and tested on the other, we used all available trials for training and testing. The accuracy of every decoder was estimated by pseudorandom resampling from the available trials 1,000 times.

In the analysis of Fig. 4, we shuffled the neurons such that the index of each neuron in PV was randomly assigned. Therefore, the spike count of every neuron remained, but its position in the vector changed.

Decision-boundary analysis. To estimate whether the mechanism that allowed decoding of one class based on the other was due to correlated selectivity or overall activity, we estimated the angle between the boundary lines. Every training sample yielded a vector of weights:

$$\text{Boundary}_{\text{class}} = \langle W_1, W_2, \dots, W_N \rangle$$

$\text{Boundary}_{\text{class}}$ was the decision boundary of one training sample in a brain region with N neurons. Every brain region had two boundaries, one for gaze and one for valence.

$$\cos(\alpha) = \frac{\text{Boundary}_{\text{valence}} \cdot \text{Boundary}_{\text{gaze}}}{|\text{Boundary}_{\text{valence}}| \cdot |\text{Boundary}_{\text{gaze}}|}$$

Each of the boundaries was sampled 1,000 times to obtain a distribution of angles. The results were presented as $\cos(\alpha)$ and not α , so zero values represent perpendicular boundaries.

Linear-regression analysis. We estimated the tuning of the neurons to valence and gaze by linear-regression analysis. The firing rate of every neuron was fitted during every time bin with one of the following equations:

$$\text{FR}_{\text{valence}} = \beta_{\text{valence}}^0 + \beta_{\text{valence}} \times \text{Valence}$$

$$\text{FR}_{\text{gaze}} = \beta_{\text{gaze}}^0 + \beta_{\text{gaze}} \times \text{Gaze}$$

Valence was 1 for air puff trials and -1 for reward trials; Gaze was 1 for EC and -1 for NEC. The regression analysis yielded for every neuron two coefficients, β_{valence} and β_{gaze} .

Scalar product of linear regression coefficients. We calculated the scalar product between β_{gaze} and β_{valence} where the vector is a vector of all neurons in a certain brain region $\beta_{\text{gaze}} = \langle \beta_{G_1}, \beta_{G_2}, \dots, \beta_{G_N} \rangle$ and $\beta_{\text{valence}} = \langle \beta_{V_1}, \beta_{V_2}, \dots, \beta_{V_N} \rangle$. The intuition behind this scalar product was that if more neurons respond in a similar direction, then the scalar product is expected to be positive and vice versa.

$$\beta_{\text{gaze}} \cdot \beta_{\text{valence}} = \sum_{i=1}^N (\beta_{G_i} \beta_{V_i})$$

We also calculated a shuffled version in which a random index was used, and hence the multiplication of the coefficients was done across two

different neurons. The shuffled scalar product was repeated 1,000 times.

Selectivity-Index. We calculated a selectivity index for each neuron in the amygdala and ACC for gaze (SIG) and valence (SIV) as follows:

$$\text{SIG} = \frac{\text{FR}_{\text{normalized EC}} - \text{FR}_{\text{normalized NEC}}}{|\text{FR}_{\text{normalized EC}}| + |\text{FR}_{\text{normalized NEC}}|}$$

$$\text{SIV} = \frac{\text{FR}_{\text{normalized Puff}} - \text{FR}_{\text{normalized Reward}}}{|\text{FR}_{\text{normalized Puff}}| + |\text{FR}_{\text{normalized Reward}}|}$$

We tested both the values of the selectivity index for valence and gaze separately, as well as the overlap between the two, and whether the selectivity is in the same direction ($\text{SIG} \times \text{SIV} > 0$).

Reporting summary

Further information on research design is available in the Nature Research Reporting Summary linked to this paper.

Data availability

All data supporting the findings of this study are available from the corresponding author upon reasonable request.

Code availability

Custom code for behavioural and electrophysiological tests is available from the corresponding author upon reasonable request.

36. Li, D., Babcock, J. & Parkhurst, D. J. openEyes: a low-cost head-mounted eye-tracking solution. In Proc. 2006 symposium on Eye tracking research & applications 95–100 (ACM, 2006).
37. Mitz, A. R., Chacko, R. V., Putnam, P. T., Rudebeck, P. H. & Murray, E. A. Using pupil size and heart rate to infer affective states during behavioral neurophysiology and neuropsychology experiments. *J. Neurosci. Methods* **279**, 1–12 (2017).
38. Meyers, E. M., Freedman, D. J., Kreiman, G., Miller, E. K. & Poggio, T. Dynamic population coding of category information in inferior temporal and prefrontal cortex. *J. Neurophysiol.* **100**, 1407–1419 (2008).

Acknowledgements We thank Y. Kfir for scientific and technical advice; E. Kahana and N. Samuel for medical and surgical procedures; D. Goldin for engineering design; and E. Furman-Haran and F. Attar for MRI procedures. This work was supported by ISF 2352/19 and ERC-2016-CoG 724910 grants to R. Paz.

Author contributions R. Pryluk and R. Paz designed the study. R. Pryluk performed all experiments. Y.S., A.H.T. and A.M. contributed to experiments. R. Pryluk developed the methods and analysed the data. A.M. and D.F. contributed to data analysis and edited the manuscript. R. Pryluk and R. Paz wrote the manuscript.

Competing interests The authors declare no competing interests.

Additional information

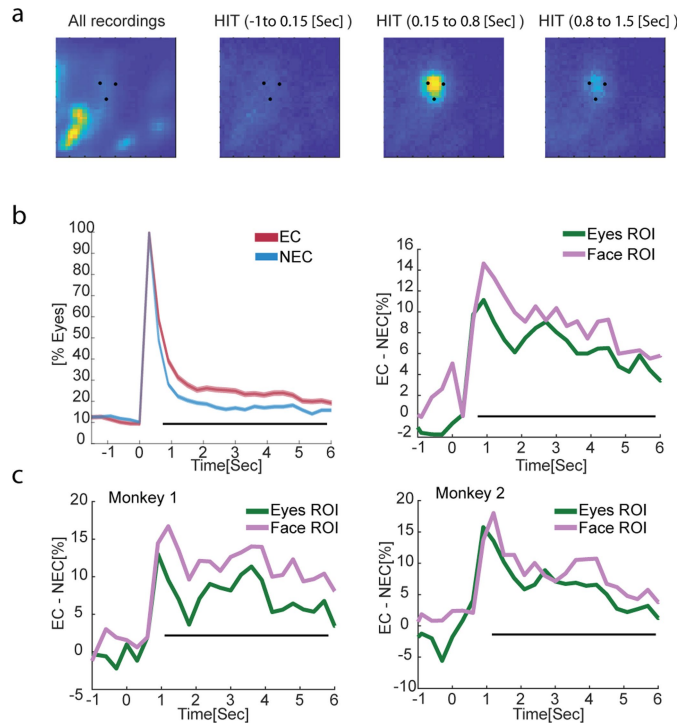
Supplementary information is available for this paper at <https://doi.org/10.1038/s41586-020-2740-8>.

Correspondence and requests for materials should be addressed to R.P.

Peer review information *Nature* thanks Jean-René Duhamel, Ziv M. Williams and the other, anonymous, reviewer(s) for their contribution to the peer review of this work.

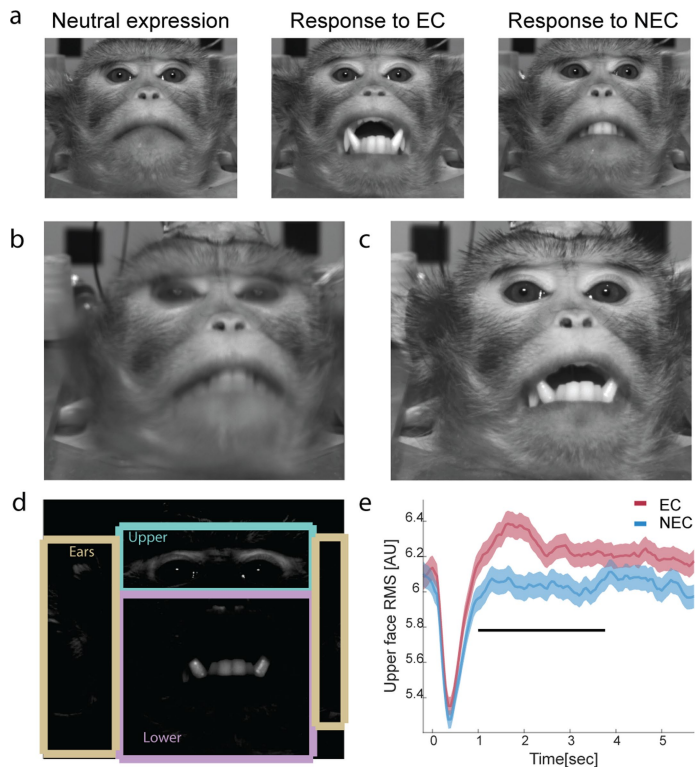
Reprints and permissions information is available at <http://www.nature.com/reprints>.

Article



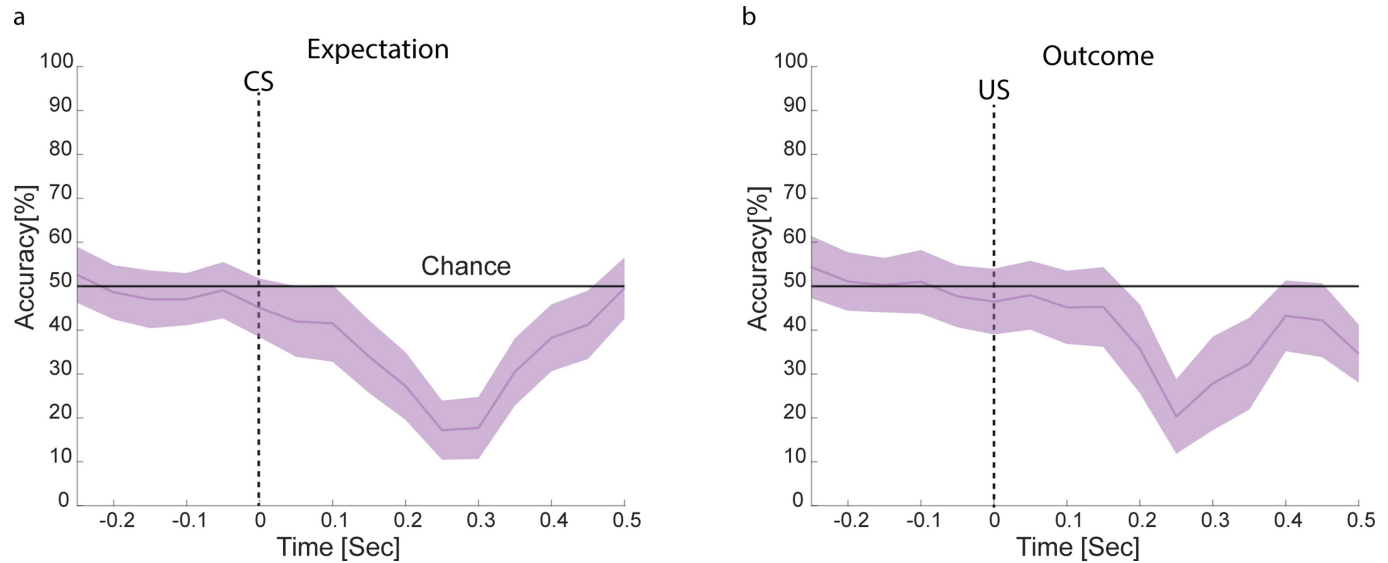
Extended Data Fig. 1 | Differential behavioural response to EC and NEC.

a, Same format as in Fig. 1f but for the all-shutter ROI (and not just face ROI). As can be seen, the monkeys looked at the face and eyes ROI mainly in the interactions with the human intruder. Left, the gaze density during all the sessions. **b**, Same format as in Fig. 1g (left), but aligned to the first time the monkeys looked to the ROI of the intruder's eyes in each trial separately. **c**, Same format as in Fig. 1g (right) separately for each monkey.



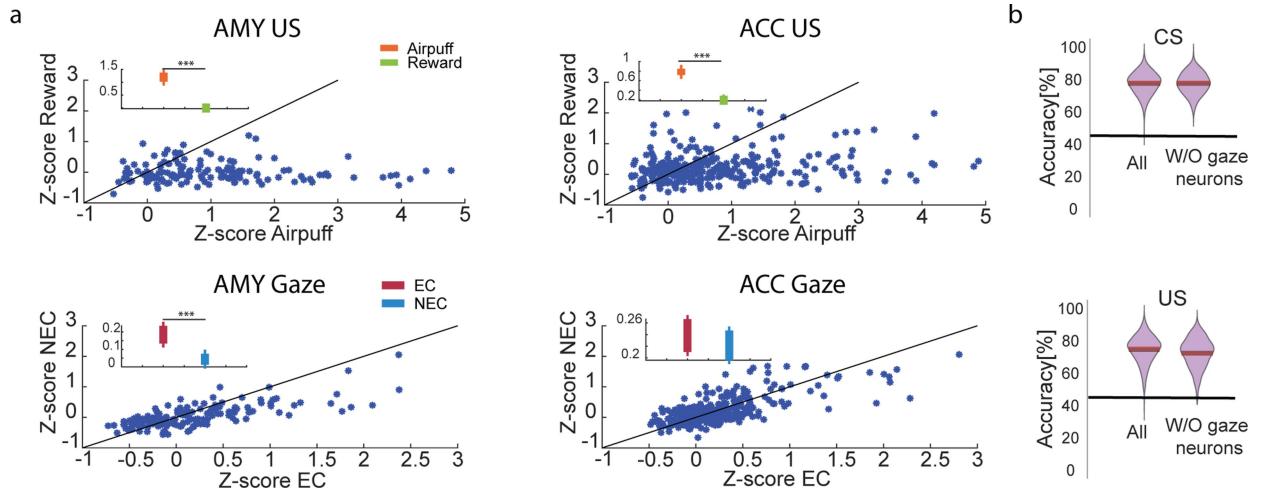
Extended Data Fig. 2 | Extracting differences in facial expression.

a, Examples of three original frames with different expressions, corresponding to the schematic in Fig. 1h. **b**, For every recording session, we averaged over all frames from the baseline period resulting in the mean image. Baseline was taken over the period before any trial when the monkey was alone in the room with a closed shutter. **c**, An example of a frame during the EC interaction. **d**, The mean frame (**b**) is subtracted from the frame in **c** during the interaction, to obtain a 'diff' (or delta) image. Three ROIs were defined manually for every day: upper face, ears and lower face. **e**, The r.m.s. of every ROI is calculated. Data are mean \pm s.e.m. The differences between EC and NEC in the upper part of the face are shown. The other parts and ROIs are shown in Fig. 1. The black line represents a significant difference; $P < 0.05$, two-sided Student's *t*-test; $n = 1,480$ trials in NEC and 1,628 trials EC.



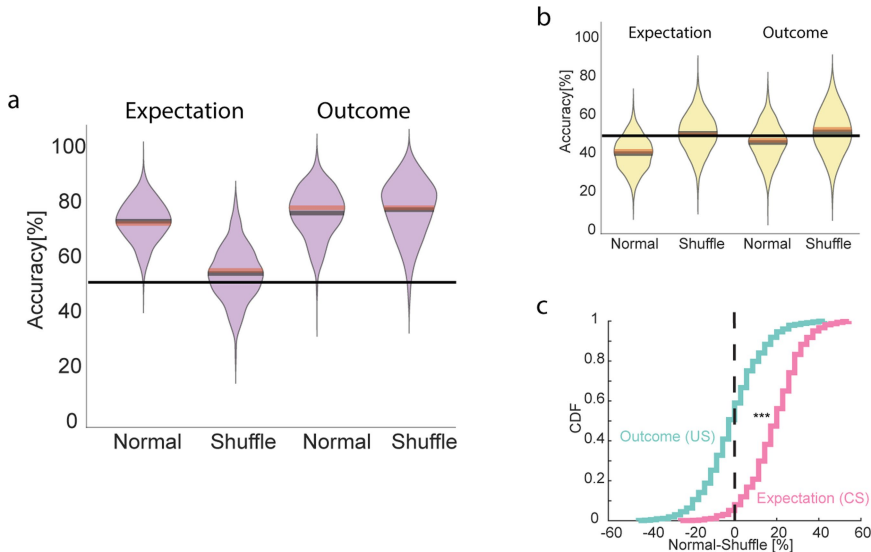
Extended Data Fig. 3 | Reversing valence directionality from NEC-EC to aversive-appetitive. **a**, Same format as in Fig. 3a, b. The population decoding accuracy is shown when training on eye gaze (NEC versus EC) and testing on

valence (aversive versus appetitive), using CS-related activity. Data are mean \pm s.d.; $n=1,000$ bootstrap replicates, $n=203$ amygdala neurons. **b**, Same as in **a** but using US-related activity.



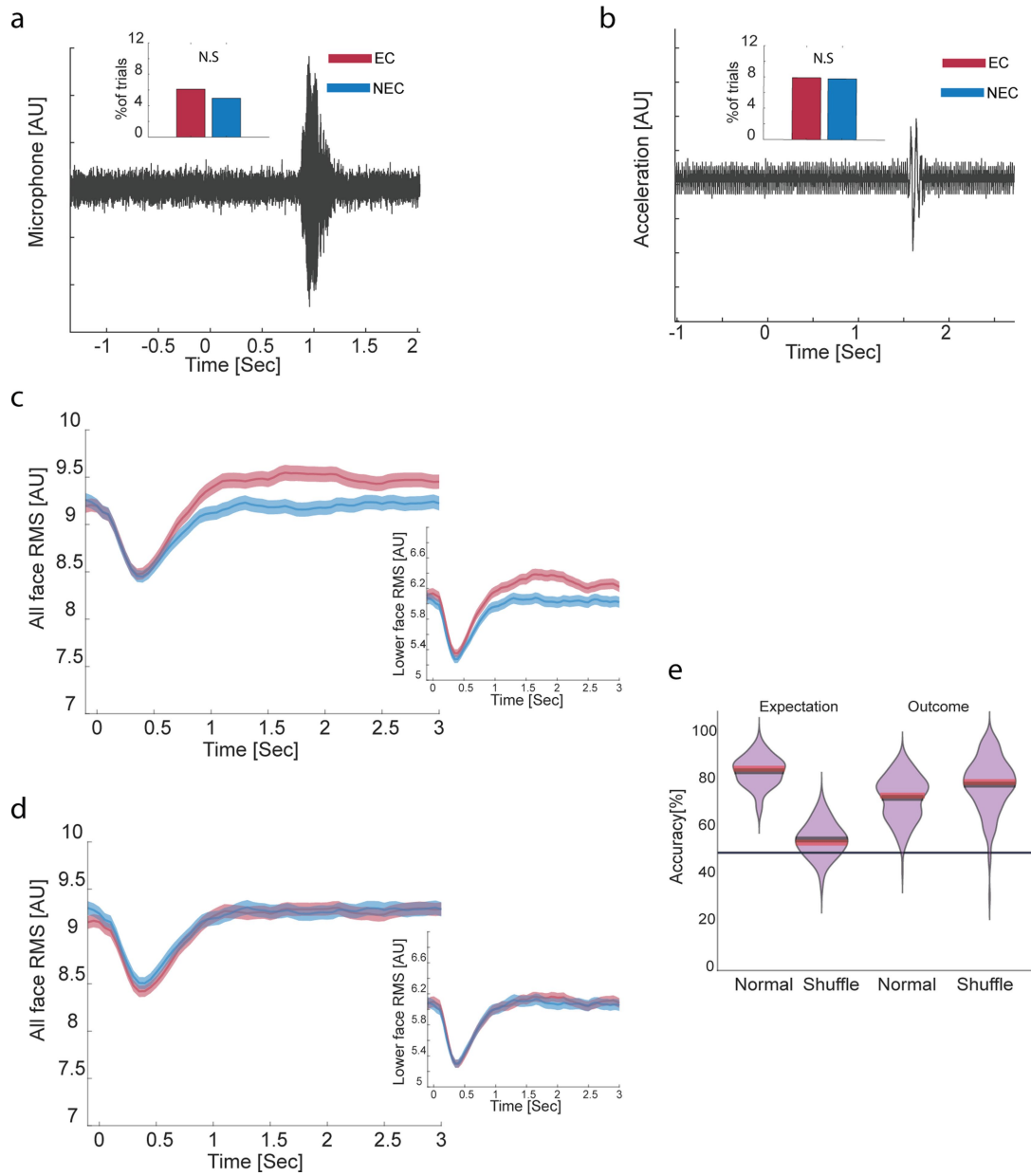
Extended Data Fig. 4 | Single-neuron activity across conditions. **a**, If overall-activity drives the successful decoding in the US epoch, we expected to find an overall change in the firing rate (increase or decrease) for gaze and US valence. Indeed, we found that there were more valence-positive neurons (increased firing rate to in response to the air puff) in the amygdala in the US epoch, and that there were more gaze-positive neurons (increased firing rate in

response to EC) in the amygdala. Inset graphs show mean \pm s.e.m.; *** $P < 1 \times 10^{-3}$; Z-test; $n = 203$ amygdala neurons, $n = 356$ ACC neurons. **b**, Decoding accuracy with and without neurons that encode gaze. Black and red lines represent the mean and median, respectively; $n = 203$ amygdala neurons, $n = 1,000$ bootstrap replicates.



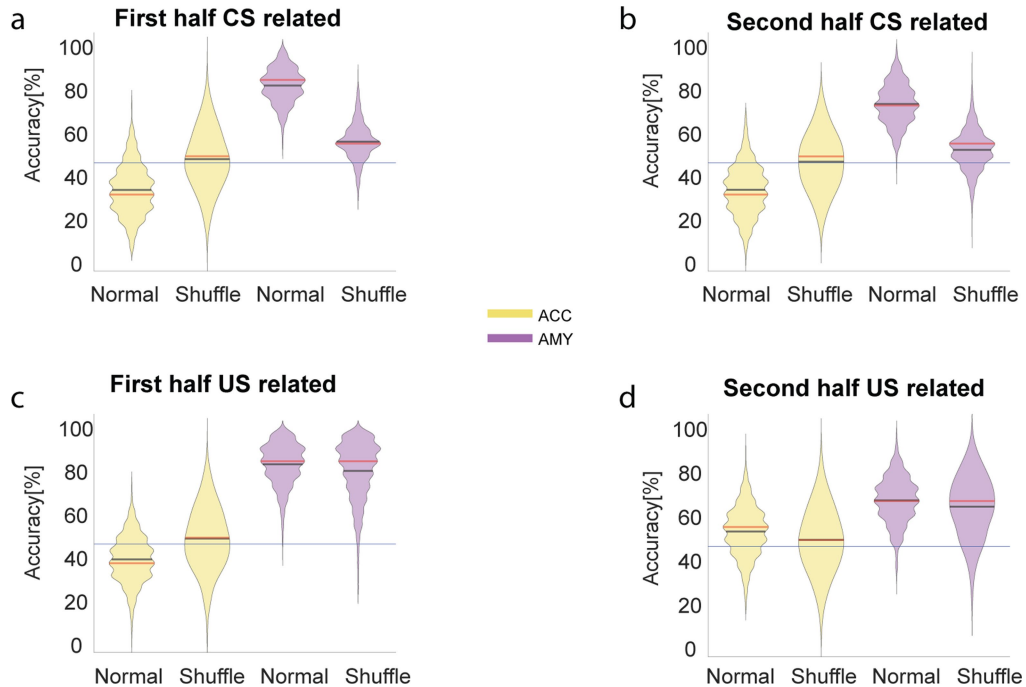
Extended Data Fig. 5 | Decoding with trial-based alignment to shutter opening. **a**, Same format as in Fig. 4h–j. Population decoding accuracy for real and shuffled amygdala neurons. Black and red lines represent the mean and median, respectively; $n=203$ amygdala neurons. **b**, Same as in **a** for ACC

activity. $n=356$ ACC neurons. **c**, Cumulative distribution of the difference in decoding accuracy between real and shuffled neurons. $***P<1\times 10^{-3}$; two-sample Kolmogorov-Smirnov test; $n=203$ amygdala neurons.



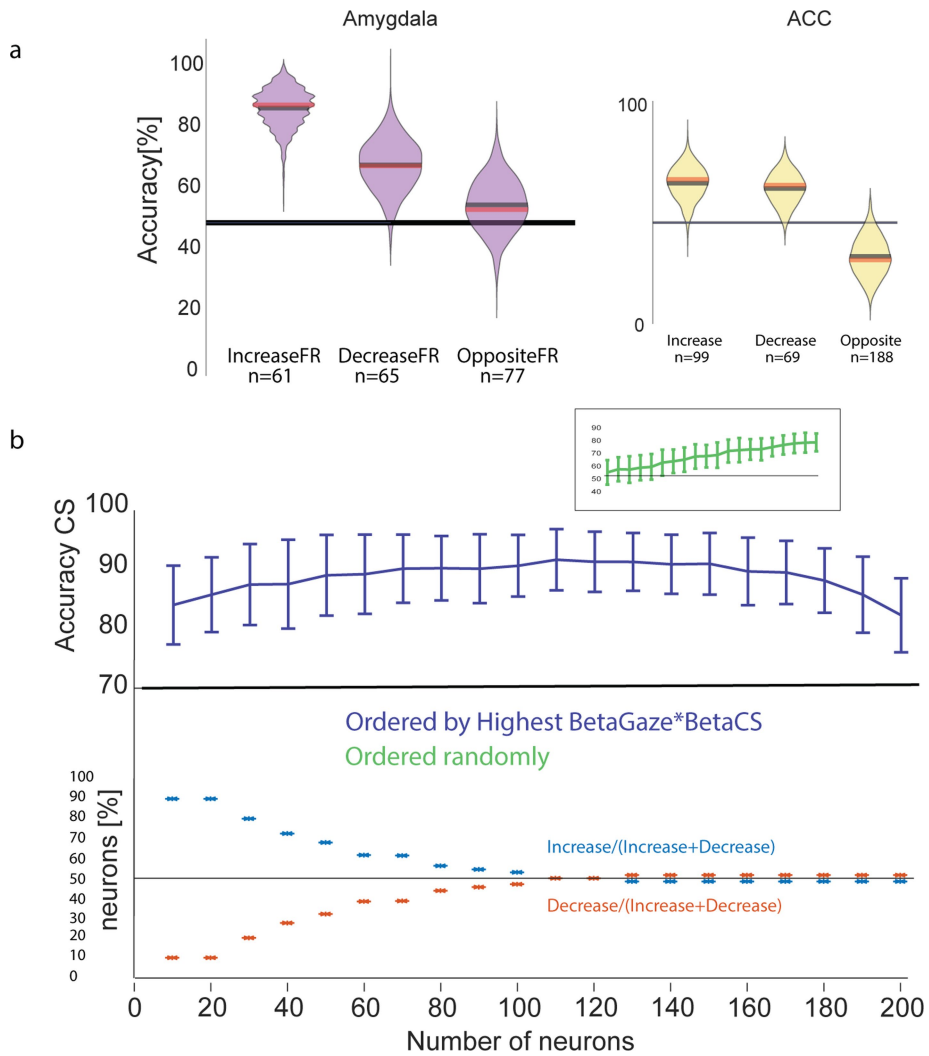
Extended Data Fig. 6 | Behavioural differences between EC and NEC do not underlie neural findings. **a**, An example of vocalizations during one HIT trial, measured using a microphone placed in close proximity to the monkey (Methods). Inset, the proportion of trials in which vocalizations occur. There was a very small proportion of trials in which vocalization occurred, and it was similar across EC and NEC trials. χ^2 test; $P=0.88$; $n=1,738$ NEC trials and $1,807$ EC trials. Owing to the low number of vocalizations, we were not able to characterize different types of vocalizations. In addition, we repeated analyses after removing trials during which vocalizations occur, and the main results were unchanged. **b**, An example of movement in one trial in response to the human intruder, measured using an accelerometer attached to the chair of the monkey (Methods). This also occurred during a small number of trials, and it was similar across EC and NEC trials. In addition, we repeated analyses after removing these trials, and the main results were unchanged. **c**, The overall

change in facial expressions between EC and NEC (as in Fig. 1i). The r.m.s. of the change between the image over the whole face (main) and only for the lower half of the face (inset), compared to the neutral expression obtained from averaging over the baseline period when the monkey was alone (Methods). Data are mean \pm s.e.m. There is a significant difference ($P<0.05$); two-sided Student's t -test; $n=1,703$ NEC trials and $1,765$ EC trials. **d**, Same as in **c** after applying the thinning method (iteratively selecting trials to obtain a similar distribution of behaviour across EC and NEC; Methods). We applied the same method also to eye movements. **e**, Decoding accuracy using only trials with similar behaviour across EC and NEC, taken after thinning as described in **d**. The results remain the same (compare to Fig. 4h). Red and black lines indicate the median and mean, respectively; $n=203$ amygdala neurons; $n=1,000$ bootstrap replicates.



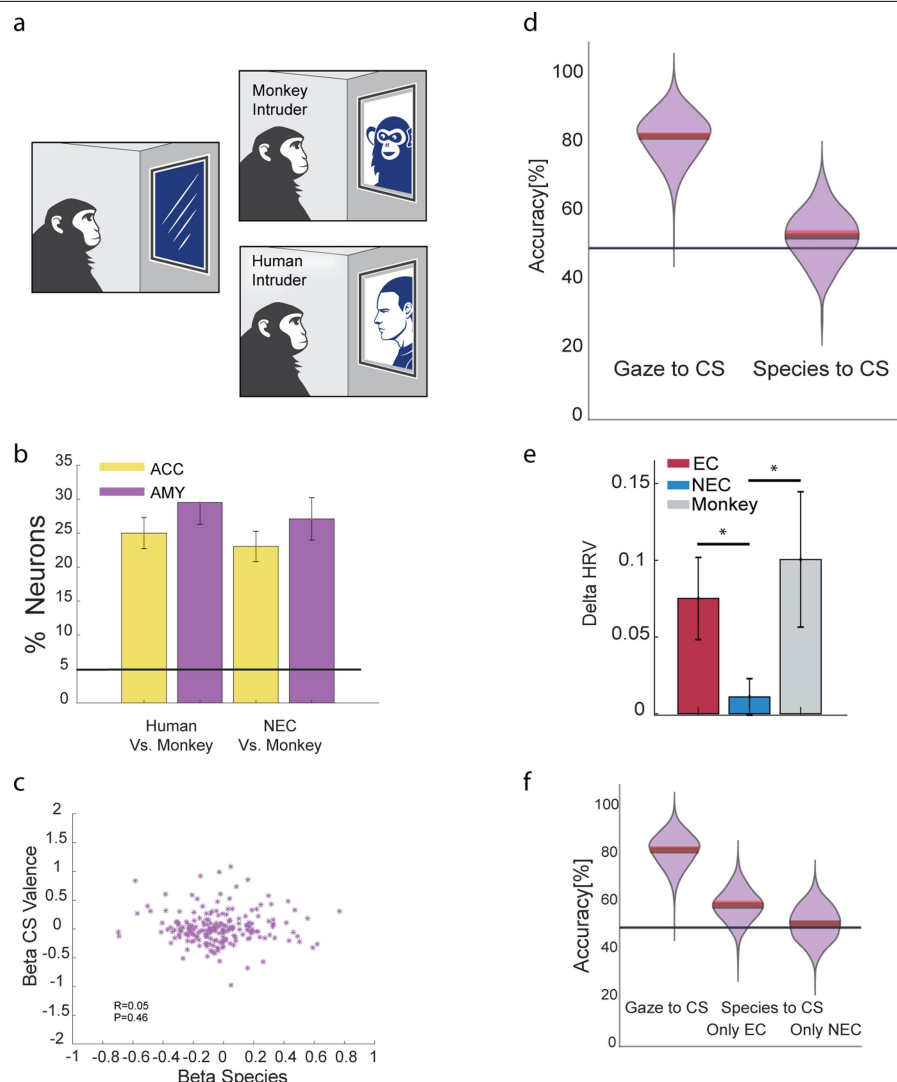
Extended Data Fig. 7 | Consistency across stimulus saliency (no within-day adaptation). a–d, Decoding accuracy was divided into the first and second half of trials and similar results were obtained. The presentation is a merged format of Fig. 4h, i. CS-related activity (a, b) or US-related activity (c, d) in the first half

(a, c) and second half (b, d) of trials is shown. Red and black lines indicate the median and mean, respectively; $n = 203$ amygdala neurons, $n = 356$ ACC neurons; $n = 1,000$ bootstrap replicates.



Extended Data Fig. 8 | Neuronal modulation. **a**, Left, we divided the amygdala neurons into three groups: the first contains neurons that increased their firing rate (FR) in response to gaze and valence (61/203, positive β values in Fig. 4a); the second group decreased FR in response to both gaze and valence (65/203, negative β values in Fig. 4a); and the third group increased FR in response to one condition and decreased in response to the other (77/203). For the first two groups, the decoding accuracy of valence based on gaze (similar analysis as in Fig. 4h for CS-related activity) was significantly higher than chance, indicating that the overall result reported in the main text is based on both increases and decreases in FR. Right, same but for ACC neurons. Red and black lines indicate the median and mean, respectively. **b**, Amygdala neurons were sorted according to degree of modulation (magnitude of $\beta_{\text{gaze}} \times \beta_{\text{valence}}$). The decoding

accuracy (mean) and its variance for increasing group size (that is, 10 neurons with highest modulation, 20 neurons... and so on) was recalculated. These values were compared to randomly chosen groups of similar size (green inset, notice the linear increase). The decoding accuracy increased until reaching a group size of 120–130 neurons; which is the number of neurons that contained the first two groups from **a** that either increased or decreased the firing rate, (but not mixed activity). Bottom, the proportion of neurons from the two groups. It can be seen that both groups contributed to the increased accuracy. These results further support the conclusion that the shared neural mechanisms are not due only to an increased firing rate, as an indication of saliency or alertness. $n = 203$ amygdala neurons.

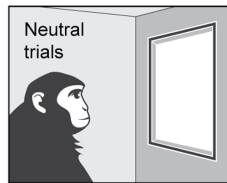
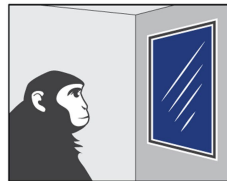
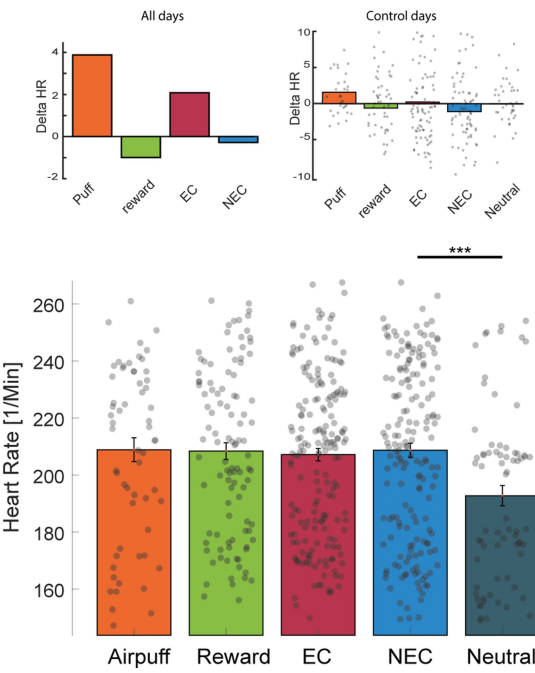


Extended Data Fig. 9 | Neurons encode species, but this coding is not shared with the valence of CS. **a**, We included monkey-intruder blocks (top) in a similar way to the HIT trials (bottom). The same neurons reported in the main analysis were recorded during the monkey–monkey interactions. For each recording session, on average two (out of six) monkeys served as intruders. All of the monkeys had lived together for several years. **b**, Neurons in the amygdala ($n = 203$), as well as in the ACC ($n = 356$), code for species and can differentiate between human and monkey intruders. Moreover, neurons differentiate between NEC human trials and monkey-intruder trials. Data are mean and s.e.m. **c**, In contrast to the findings in Fig. 4a, there was no significant correlation (Pearson's correlation, $r = 0.05$, $P = 0.45$, $n = 203$) between β_{species} and $\beta_{\text{CSvalence}}$, strongly arguing against a correlated-selectivity mechanism between

species and CS. **d**, Decoding accuracy of CS valence after training the decoder to differentiate species, was not different from chance level and significantly smaller than the decoding accuracy of CS valence based on gaze. Red and black lines indicate the median and mean, respectively. $n = 203$ amygdala neurons; $n = 1,000$ bootstrap replicates. **e**, Differences in heart-rate variability between monkey-intruder and NEC trials (as shown for EC and NEC trials (Fig. 1k)).

* $P < 0.05$; two-sided Student's t -test; $n = 1,703, 1,765$ and $1,620$ trials in NEC, EC and monkey trials.

f, Despite differences in heart-rate variability (e), the findings in d remained similar when using either only EC or only NEC trials of the human intruder ($n = 203$ amygdala neurons). Red and black lines indicate the median and mean, respectively.

a**b**

Extended Data Fig. 10 | NEC trials are different from neutral trials. **a**, We included neutral trials, in which the opening of the shutter (CS) is followed by nothing. **b**, The heart rate was significantly lower in neutral trials compared to all others types of trial and, specifically, it was lower than in NEC trials. Top left, difference in heart rate, same as in Fig. 1.j. Top right, difference in heart rate in the control days that included neutral trials, showing the same trend for all

types of trial and no modulation for neutral trials. Together, these results indicate that the NEC trials were not salience-free, but rather highly salient in a different manner than the EC trials. $n=1,703, 1,765, 1,620, 1,352$ and 712 trials for NEC, EC, monkey, reward and air puff trials, respectively. Data are mean \pm s.e.m., *** $P < 1 \times 10^{-3}$; two-sided Student's t -test.

Reporting Summary

Nature Research wishes to improve the reproducibility of the work that we publish. This form provides structure for consistency and transparency in reporting. For further information on Nature Research policies, see our [Editorial Policies](#) and the [Editorial Policy Checklist](#).

Statistics

For all statistical analyses, confirm that the following items are present in the figure legend, table legend, main text, or Methods section.

n/a Confirmed

- The exact sample size (n) for each experimental group/condition, given as a discrete number and unit of measurement
- A statement on whether measurements were taken from distinct samples or whether the same sample was measured repeatedly
- The statistical test(s) used AND whether they are one- or two-sided
Only common tests should be described solely by name; describe more complex techniques in the Methods section.
- A description of all covariates tested
- A description of any assumptions or corrections, such as tests of normality and adjustment for multiple comparisons
- A full description of the statistical parameters including central tendency (e.g. means) or other basic estimates (e.g. regression coefficient) AND variation (e.g. standard deviation) or associated estimates of uncertainty (e.g. confidence intervals)
- For null hypothesis testing, the test statistic (e.g. F , t , r) with confidence intervals, effect sizes, degrees of freedom and P value noted
Give P values as exact values whenever suitable.
- For Bayesian analysis, information on the choice of priors and Markov chain Monte Carlo settings
- For hierarchical and complex designs, identification of the appropriate level for tests and full reporting of outcomes
- Estimates of effect sizes (e.g. Cohen's d , Pearson's r), indicating how they were calculated

Our web collection on [statistics for biologists](#) contains articles on many of the points above.

Software and code

Policy information about [availability of computer code](#)

Data collection

- 3-tesla MRI scanner: (MAGNETOM Trio, Siemens).
 - Electrophysiological recording was done using Alpha Lab Pro (V1), Alpha Omega.
 - Offline spike sorting was done using Plexon offline sorter (V3.0,Plexon Inc).

Data analysis

- Open Eyes (V1, Babcock et al, ACM, 2006); All codes were custom made using Matlab 2016a

For manuscripts utilizing custom algorithms or software that are central to the research but not yet described in published literature, software must be made available to editors and reviewers. We strongly encourage code deposition in a community repository (e.g. GitHub). See the Nature Research [guidelines for submitting code & software](#) for further information.

Data

Policy information about [availability of data](#)

All manuscripts must include a [data availability statement](#). This statement should provide the following information, where applicable:

- Accession codes, unique identifiers, or web links for publicly available datasets
- A list of figures that have associated raw data
- A description of any restrictions on data availability

All data supporting the findings of this study are available from the corresponding author upon reasonable request.

Field-specific reporting

Please select the one below that is the best fit for your research. If you are not sure, read the appropriate sections before making your selection.

- Life sciences Behavioural & social sciences Ecological, evolutionary & environmental sciences

For a reference copy of the document with all sections, see nature.com/documents/nr-reporting-summary-flat.pdf

Life sciences study design

All studies must disclose on these points even when the disclosure is negative.

Sample size	No power calculation were used to predetermine sample size. Two monkeys were used for electrophysiological recordings, as this is customary in monkey electrophysiology to balance power and animal use.
Data exclusions	Data was not excluded from the analysis.
Replication	2 monkeys were used and resampling methods were applied.
Randomization	All neurons were tested against all behavioral conditions in a blind manner.
Blinding	Blinding is done as spike sorting is blind to the timing of the stimuli.

Reporting for specific materials, systems and methods

We require information from authors about some types of materials, experimental systems and methods used in many studies. Here, indicate whether each material, system or method listed is relevant to your study. If you are not sure if a list item applies to your research, read the appropriate section before selecting a response.

Materials & experimental systems	Methods
n/a	Involved in the study
<input checked="" type="checkbox"/>	<input type="checkbox"/> Antibodies
<input checked="" type="checkbox"/>	<input type="checkbox"/> Eukaryotic cell lines
<input checked="" type="checkbox"/>	<input type="checkbox"/> Palaeontology and archaeology
<input type="checkbox"/>	<input checked="" type="checkbox"/> Animals and other organisms
<input checked="" type="checkbox"/>	<input type="checkbox"/> Human research participants
<input checked="" type="checkbox"/>	<input type="checkbox"/> Clinical data
<input checked="" type="checkbox"/>	<input type="checkbox"/> Dual use research of concern
n/a	Involved in the study
	<input checked="" type="checkbox"/> ChIP-seq
	<input checked="" type="checkbox"/> Flow cytometry
	<input type="checkbox"/> MRI-based neuroimaging

Animals and other organisms

Policy information about [studies involving animals](#); [ARRIVE guidelines](#) recommended for reporting animal research

Laboratory animals	Two male macaca fascicularis (5–6 years old, 4–8 kg)
Wild animals	The study did not involve wild animals.
Field-collected samples	The study did not involve samples collected in the field.
Ethics oversight	All procedures were approved and conducted in accordance with the regulations of the Weizmann Institute Animal Care and Use Committee (IACUC), following NIH regulations and with AAALAC accreditation

Note that full information on the approval of the study protocol must also be provided in the manuscript.